

Effects of Cu doping on the structural, optical and electrical characterizations of spray-deposited Ni-O thin films

G. Rihia, M. Ghougali, A. Beggas *, M. Mimouni, M. S. Mahboub
LEVRES Laboratory, University of El Oued, 39000 El Oued, Algeria

The study involved depositing nickel oxide samples on well-cleaned substrates of ordinary glass by employing the spray pyrolysis method. The main objective was to examine how different concentrations of copper-doping impact nickel oxide sample's structural, electrical, and optical characteristics. The XRD patterns of the copper-doped nickel oxide indicated that increasing copper concentration levels led to improved film crystallinity. The crystal sizes and strain of the films were evaluated using Williamson-Hall analysis. The study also discussed the optical properties, with a focus on using transmittance data to assess the optical bandgap energy and Urbach energy, which are important optical parameters. The increase in electrical conductivity to its maximum value can be interpreted via the rise in the carrier concentration in the prepared samples. The NiO:Cu thin film exhibits interesting electrical conductivity due to its low sheet resistance. NiO:Cu film has the potential for use in various electronic and optoelectronic devices because of its optical bandgap, significant transparency in the visible spectrum, and excellent electrical conductivity.

(Received October 31, 2024; Accepted February 4, 2025)

Keywords: Nickel oxide, XRD patterns, NiO Thin films, Optical properties, Electrical conductivity

1. Introduction

Nickel oxide (NiO) is a widely studied and gained significant interest due to its low-cost and diverse applications, including its use as a catalyst, transparent conducting oxide, photodetectors, electrochromic material, gas sensors, supercapacitors, photo-electrochemical cells, and various optoelectronic equipment [1-9]. NiO is a transparent p-type semiconductor with an optical bandgap energy ranging from 3.45 eV to 3.85 eV [10], making the bandgap worthy of adjusting the state-level energy of NiO. Various approaches have been employed for the synthesis of NiO: Cu nanostructure materials, including the thermal evaporation, the pulsed laser ablation, sputter-ing, electrodeposition, and sol-gel process process, etc. [11-16]. Amongst these processes, spray pyrolysis [17] offers many favors such as the considerable purity of raw materiality and a homogeneous sol consequently easy to deal and control with. To improve the main properties of NiO samples, many researchers have investigated the impact of various dopants including Al [18], Fe [19], Cu [20, 21], Mn [19, 22], and Zn [22] on the different characteristics of these samples. Nevertheless, there has been relatively little research on copper (Cu)-doped NiO thin films p-type semiconductors.

This work used the spray pyrolysis method to fabricate NiO: Cu thin layers with different copper doping concentrations. The structural characteristics of the copper-doped nickel oxide samples were analyzed. Additionally, the transmittance spectra of the NiO: Cu films were measured in the wavelength range of 200-900 nm. The optical bandgap was also calculated as a function of copper content in the samples.

* Corresponding author: azzeddine-beggas@univ-eloued.dz
<https://doi.org/10.15251/DJNB.2025.201.139>

2. Experimental procedure

2.1. Sample preparation

A spray pneumatics technique was used to synthesize NiO: Cu thin films onto extremely clean glass substrates. For all the samples in the paper, nickel nitrate hexahydrate and copper (II) nitrate were dissolved in deionized water as solvent and HCl was used as a stabilizing agent. The copper nitrate concentration and precursor molarity were maintained at 0.20 mol L^{-1} . The two solutions were mixed in specific volume ratios to achieve the following atomic ratios of Cu/ (Ni + Cu): 0, 3, 6, 9, and 12. The resulting mixed solution was agitated at $60 \text{ }^\circ\text{C}$ for 30 min to get a pure and homogenous solution, and then the mixture was cooled to room temperature. The glass surfaces were cleaned with acetone and deionized water, followed by drying with an ordinary hair dryer.

2.2. Deposition of thin films

The precursor solution mixture was intermittently sprayed on ordinary glass substrate at $480 \text{ }^\circ\text{C}$ during 2 minutes, so that the substrate is allowed to maintain its temperature. This was done by an air nebulizer system where the liquid was transformed into a spray stream consisting of regular and fine droplets. During the precursor solution spray falls onto the surface of the hot substrate and the film is gradually formed.

2.3. Characterization techniques

In order to verify the samples structure, the (XRD) spectra of the NiO: Cu have been measured at room temperature. It was accomplished with the use of a (BRUKER-AXS-8D) diffractometer with Cu $K\alpha$ radiation ($\lambda = 0.15406 \text{ nm}$) working at (40 kV and 40 mA) in the scan region of (2θ) from 30 to 100° . An ultraviolet-visible spectrophotometer (Perkin-Elmer Lambda 25) was used to measure the spectral dependence of NiO: Cu transmittance (T) and wavelength in the $200\text{-}900 \text{ nm}$ range.

3. Results and discussion

3.1. X-ray diffraction analysis

This study aims to elucidate the structure of NiO: Cu thin layers deposited with varying copper contents, XRD has been employed. The XRD patterns of all the samples are presented in Figure 1. It is evident from the figure that each pattern displays a diffraction peak around $2\theta \sim 37^\circ$, corresponding to the (111) preferred orientation, along with additional peaks identified as (200), (220), and (311). These findings are consistent with the Joint Committee on Powder Diffraction Standards (JCPDS: card number. 89-7130) within the (Fm3m) space group, consistent with previous reports [23, 24].

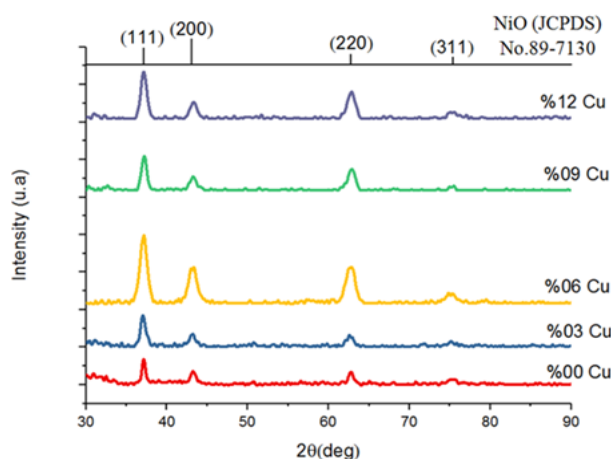


Fig. 1. XRD of NiO:Cu samples deposited on glass substrates with varying copper concentrations.

These peak positions indicate that the samples have a natural cubic crystal structure, consistent with other reports [11, 12]. One may observe that there are no peaks in the XRD pattern corresponding to Cu doping present, suggesting that the copper atoms were successfully incorporated into the NiO host lattice. Indeed, low-level impurity doping does not cause the appearance of new XRD peaks but rather shifts the host material lattice parameters. The aforementioned shift can be attributed to the distortion that occurs as a consequence of the dopant's insertion in the lattice [9]. A significant increase in the intensity of the peak at (111) lattice plane was observed with 6% Cu doping, indicating an improvement of the crystallinity at this concentration. This improvement is attributed to the substitution of Ni²⁺ ions (R Ni²⁺ ≈ 0.69 Å) by Cu²⁺ ions (R Cu²⁺ ≈ 0.73 Å), which reduces the stress in the lattice and promotes better crystallization [9, 25]. Williamson-Hall analysis was used to determine crystal size and lattice strain in Cu-doped NiO films. Based on the Williamson and Hall relationships it was supposed that both the size and the strain broadening profiles are Lorentzian. In light of this supposition, a mathematical relationship was developed linking the full width at half-maximum intensity β , the mean crystal size D , and microstrain ϵ according to the following formula (3.1) [25]:

$$\beta \cos\theta = \frac{k\lambda}{D} + 4\epsilon \sin\theta \quad (3.1)$$

In this context, k stands for the shape factor, λ represents the incident radiation X-ray wavelength (0.15404 nm) used in the scanning process of the samples, and β corresponds to the (FWHM) of the diffraction peak, and θ is the diffraction peak angle.

Figure 2. illustrates the plot of $\beta \cos\theta$ as a function of $4 \sin\theta$, where the microstrain value is determined from the slope of the graph, and the crystallite size is obtained by the intercept of the straight line with the axis of ordinates. In the event that the points in the W-H graph are dispersed, that is to say, if $\beta \cos\theta$ is not a monotone function of $4 \sin\theta$, the widening is called anisotropic [26]. The average values of crystallite size and strain are summarized in Table 1. The crystallite size ranges on average between 22.45 and 39.08 nm. Figure 3. represents the relation between crystallite size and microstrain at various copper doping levels. Pure NiO layers displayed a crystallite size (D) of 39.08 nm, which gradually reduced to 24.46 nm as the Cu concentration increased to 3% and 6%. Higher doping levels led to a reduction in crystallite size (D). This decrease can be explained by the incorporation of copper atoms, which act as obstacles to grain boundary movement, thereby hindering the grain growth. However, the microstrain ϵ variation followed a different trend as shown in Figure 3. This divergence can be assigned to the difference in ionic radii that exist inter the doping atoms and NiO, leading to changes in microstrain.

Table 1. Structural parameters of NiO:Cu samples at varying copper contents.

Cu (%)	0	3	6	9	12
D(nm)	39.08	28.68	22.45	27.22	24.46
ϵ (%)	0.112	0.194	0.316	0.240	0.215

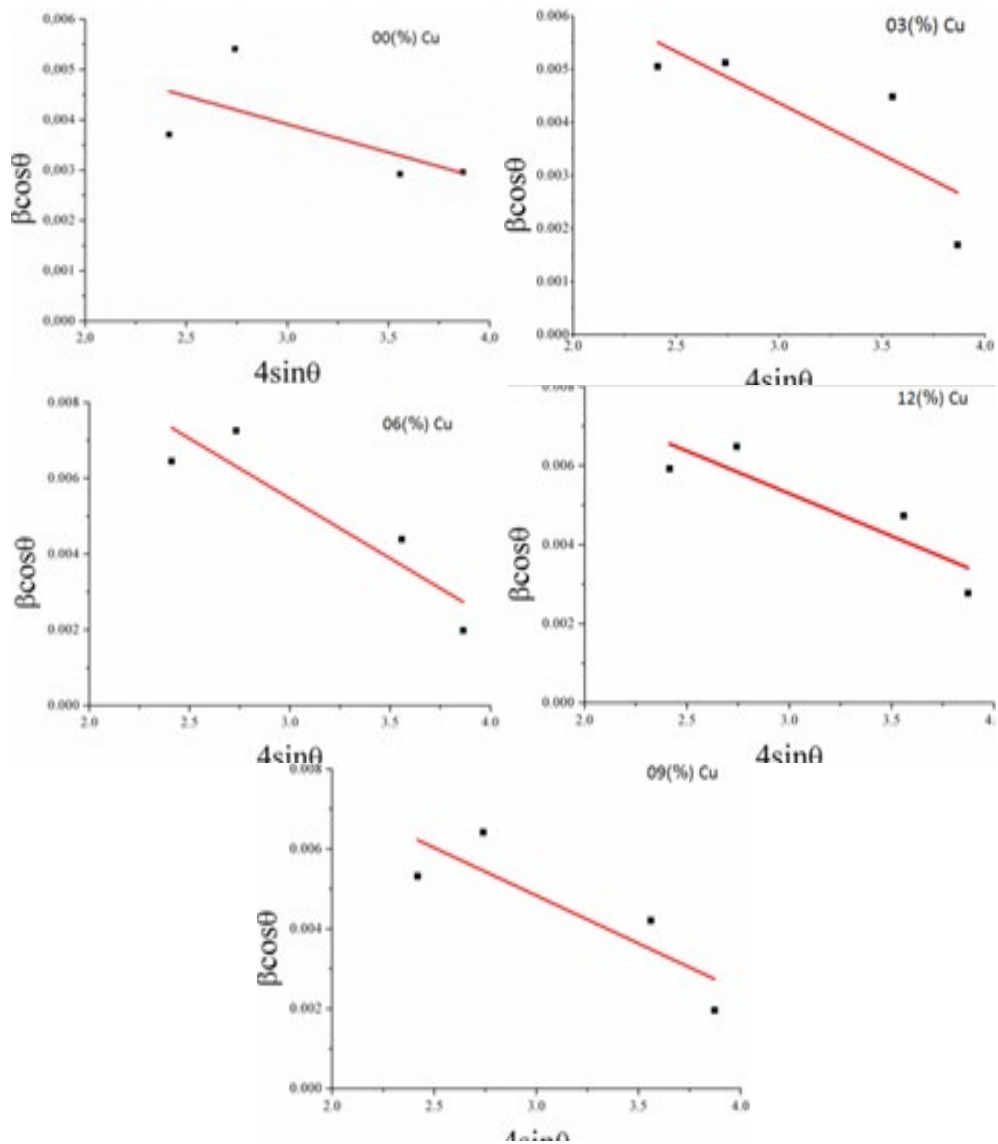


Fig. 2. Williamson-Hall plot approach.

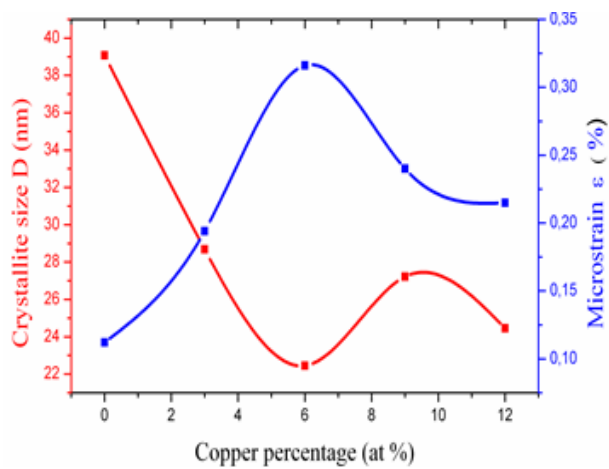


Fig. 3. The variation in crystallite size and microstrain of NiO:Cu layers in relation to copper concentration.

3.2. Optical properties

In the transmittance analysis shown in Figure 4, the NiO:Cu films exhibited a remarkable transmittance rate of 80% at a copper concentration of 3%, averaging over the 300 to 900 nm wavelength range. The absorption coefficient is in relationship with the incidence photon energy by the expression given by equation (3.2) [27]:

$$\alpha h\nu = C(h\nu - E_g)^n \quad (3.2)$$

where, C is a constant, ν denotes the incidence irradiation frequency, h is the constant of Planck, and n is a numerical value that defines the optical processes, which is equal to 0.5 in the case of a directly allowed band transition. The photon energy $h\nu$ is given by the expression $h\nu = 1240/\lambda$ (nm) in electron volts (eV), E_g represents the bandgap of the semiconductor. The bandgap values of the NiO:Cu layers are presented in Table 2.

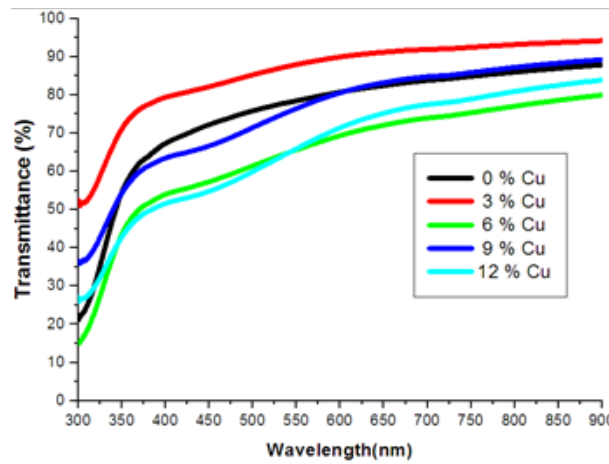


Fig. 4. Transmittance versus wavelength for NiO: Cu layers at various copper concentrations.

For a pure NiO layer, the E_g value is 3.60 eV, which is in good agreement with the reported value for the bulk material [28]. It is evident that the calculated values of E_g exhibit a decline with an increase in copper content. The observed variation in E_g can be attributed to the effect of several contributing effects, including the thickness of the film, strain, size of crystallite, and the existence of any impurities within the samples. These observations are supported by the findings of reference [29]. The Urbach energy (E_u) is a valuable parameter for evaluating structural disorder in a material, as it characterizes the tails of localized states in the bandgap [30]. To estimate the Urbach energy, one can utilize Equation (3.3). The E_u values are determined of the inverse of the curve slope that is plotted as $(\ln(\alpha))$ versus $(h\nu)$ [31].

$$\ln(\alpha) = \frac{1}{E_u}(h\nu) + \ln(\alpha_0) \quad (3.3)$$

where, (α_0) represents the pre-exponential factor, while the quantity $(h\nu)$ denotes the energy of a photon.

As detailed in Table 2, the calculated values of E_u range from 0.523 to 0.935 eV. The data presented indicate that the value of E_u rises with higher copper doping levels. This phenomenon can be justified by the figuration of localized states that occurs as a result of the doping ions being incorporated within the optical bandgap. While the presence of crystal defects may also serve as a contributing factor to the figuration of localized states in forbidden bandgap, the influence of copper doping is more pronounced in this regard.

Table 2. The bandgap and Urbach energies values of the NiO:Cu layers.

Cu (%)	0	3	6	9	12
E _g (eV)	3.6	3.53	3.57	3.46	3.43
E _U (eV)	0.523	0.591	0.644	0.782	0.935

Figure 5 illustrates the variation in E_g and E_U values versus Cu doping percentages, an increase of Urbach energy (E_U) values with rising Cu doping percentages is noticed, despite a decrease in crystalline defects. It is evident from the latter figure that E_g and E_U exhibit opposing trends. The shift in E_g values observed for all the samples is corroborated by its elevated E_U value, which substantiates the enhanced disorderliness of these films.

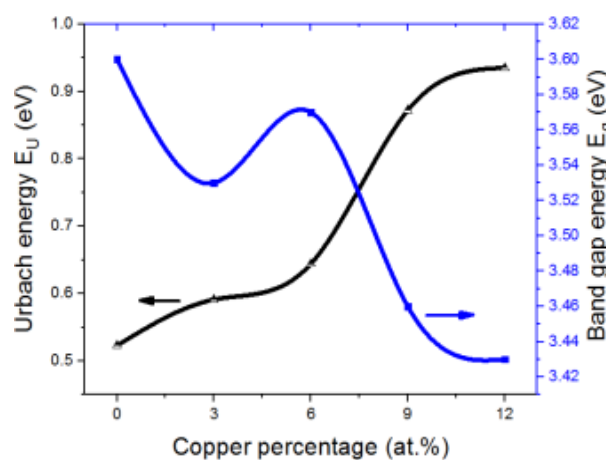


Fig. 5. Bandgap and Urbach energies of NiO: Cu layers as a function of Cu concentration.

3.3. Electrical properties

The electrical properties of NiO: Cu thin layers were examined through the four-point linear probe method. The electrical conductivity (σ) of the films was found by employing the following formula (3.4), as proposed by [25]:

$$\sigma = \frac{1}{dR_{sh}} \quad (3.4)$$

where: d represents the film thickness, and R_{sh} denotes the sheet resistance.

Figure 6 demonstrates the variation in electrical conductivity (σ) of NiO:Cu thin layers with increasing copper content. The films exhibit excellent conductivity, reaching a peak value of $2.916 (\Omega \text{ cm})^{-1}$ at a 12% copper concentration. The observed enhancement in conductivity is associated with an increase in carrier concentration. As documented by Patil et al. [32], the surge in electrical conductivity correlates with elevated activation energy, which is linked to augmented film thickness. This phenomenon is influenced by a multitude of experimental parameters, including the composition of the spraying solution, the spray rate, and the substrate cooling process at the stage of decomposition.

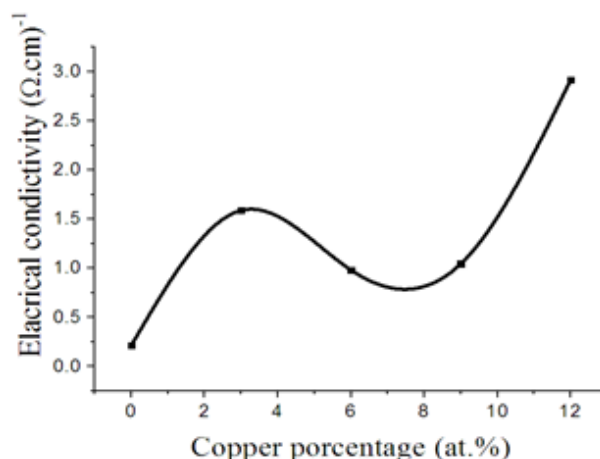


Fig. 6. Graph of the electrical conductivity versus copper concentration.

4. Conclusions

Spray pyrolysis method was successfully utilized to fabricate NiO:Cu samples with different copper concentrations onto glass substrates. All deposited films crystallized in a cubic crystallization, showing a pronounced orientation along the (111) plane. The smallest observed crystallite size was 22.45 nm at a copper content of 6%. A significant improvement in the crystallinity of the films was noted at 6% copper concentration, where the (111) peak at 37.1° appeared prominently sharp. The film produced at this concentration demonstrated an intense and well-defined diffraction peak, confirming an enhancement in peak intensity relative to the other layers. The bandgap values of the NiO:Cu layers ranged from 3.43 eV to 3.6 eV, with Urbach energy values varying between 0.523 eV and 0.935 eV. The NiO:Cu films exhibited high optical transmittance of 80% and a conductivity of 1.9102 (Ω cm)⁻¹, indicating their potential suitability for optoelectronic applications. They are particularly promising for use as a window layer in solar cell technologies.

References

- [1] M. A. Abbasi, Z. H Ibutoto, A. Khan, O. Nur, M. Willander, *Materials Letters* **108**, 149-152 (2013); <https://doi.org/10.1016/j.matlet.2013.06.083>.
- [2] M. Dirwin, D. B. Buchholz, A. W Hains, R. P Chang, T. J Marks *Proceedings of the National academy of Sciences*, **105**(8), 2783-2787 (2008); <https://doi.org/10.1073/pnas.071199010>.
- [3] M. Ghougali, O. Belahssen, A. Chala, *Journal of Nano- and electronic Physics Optical Materials* **119**, 111369 (2016); [https://doi.org/10.21272/jnep.8\(4\(2\)\).04059](https://doi.org/10.21272/jnep.8(4(2)).04059).
- [4] J. Kim, J. H. Yun, Y. C Park, W. A. Anderson, *Materials Letters* **132**, 322-326 (2012); <https://doi.org/10.1016/j.matlet.2012.01.144>.
- [5] M. J. Park, J. Y. Jung, S. M. Shin, J. W. Song, Y. H. Nam, D .H. Kim, J. H. Lee, *Thin Solid Films* **599**, 54-58 (2016); <https://doi.org/10.1016/j.tsf.2015.12.062>.
- [6] K. CWang, P. S Shen, M. H Li, S. Chen, M. W. Lin P. Chen T. F. Guo, *ACS applied materials & interfaces* **6**(15), 11851-11858. (2014); <https://doi.org/10.1021/am503610u>
- [7] J. H Yun, J. Kim, Y. C Park, S. J Moon, W. A Anderson, *Thin Solid Films*, **547**, 17-21(2013); <https://doi.org/10.1016/j.tsf.2013.05.072>.
- [8] S. Ahn, A. H. T. Le, S. Kim, et al, *Materials Letters*, **132**, 322-326 (2014) ; <https://doi.org/10.1016/j.matlet.2014.06.074>.
- [9] M. Ghougali, O. Belahssen, A. Chala, *Journal of nano- and electronic physics*, **T.9, № 3.**, 03043 (2017); [https://doi.org/10.21272/jnep.9\(3\).03043](https://doi.org/10.21272/jnep.9(3).03043).

- [10] D. Zaouk, Y. Zaatari, R. Asmar, J. Jabbour, *Microelectronics journal*, **37**(11), 1276-1279 (2006); <https://doi.org/10.1016/j.mejo.2006.07.024>.
- [11] H. Ahmoum, G. Li, S. Belakry, M. Boughrara, M. S. Su'ait, M. Kerouad, Q. Wang, *Materials Science in Semiconductor Processing*, **123**, 105530 (2021); <https://doi.org/10.1016/j.mssp.2020.105530>
- [12] M. M. A Hussein, *INAE Letters*, **2**(1), 35-39. (2017); <https://doi.org/10.1007/s41403-017-0019-7>
- [13] T. A Alrebdi, H. A Ahmed, S. H Alrefae, R. A. Pashameah, A. Toghan, A. M. Mostafa, F. Alkallas, R. A. Rezk., *Journal of Materials Research and Technology*, **20**, 4356-4364 (2022); <https://doi.org/10.1016/j.jmrt.2022.08.165>
- [14] P. Ravikumar, B.Kisan, A. Perumal *Journal of Magnetism and Magnetic Materials*, **418**,. 86-91(2016); <https://doi.org/10.1016/j.jmmm.2016.02.091>.
- [15] H. Aydin, S. A Mansour, C. Aydin, A. A. Al-Ghamdi, O. A. Al-Hartomy, F. El-Tantawy, F. Yakuphanoglu, *Journal of sol-gel science and technology*, **64**, 728-733(2012); <https://doi.org/10.1007/s10971-012-2909-1>.
- [16] N. Aswathy, J. Varghese, R.V. Kumar, *The European Physical Journal Plus* **137**, 1344. (2022); <https://doi.org/10.1016/j.matchemphys.2022.125916>
- [17] U. Alver, H. Yaykaşlı, S. Kerli, A. Tanrıverdi, *International Journal of Minerals, Metallurgy and Materials*, **20**, 1097-1101 (2013); <https://doi.org/10.1007/s12613-013-0839-8>.
- [18] N. Srinivasa, H. Mahesh, B. Angadi, *Advances in Natural Sciences: Nanoscience and Nanotechnology* **15**(4), 045009 (2024); <https://doi.org/10.1088/2043-6262/ad7c19>
- [19] N. Aswathy, J. Varghese, S. R Nair, R. V Kumar, *Materials Chemistry and Physics*, **282**, 125916 (2022); <https://doi.org/10.1016/j.matchemphys.2022.125916>.
- [20] M. Aftab, M. Butt, D. Ali, F. Bashir, T. M. Khan, *Optical Materials*, **119**, 111369. (2021); <https://doi.org/10.1016/j.optmat.2021.111369>.
- [21] A. Javadian, M. Fadavieslam, *Journal of Materials Science: Materials in Electronics*, **33**(30), 23362-23374 (2022); <https://doi.org/10.1007/s10854-022-09098-5>.
- [22] M. E. Begum, M. B. Islam, M. H Ara, A. Doris, M. A Kaiyum, M. Rasadujjaman, *Heliyon*, **10**(1), 24244 (2024); <https://doi.org/10.1016/j.heliyon.2024.e24244>.
- [23] A. Al-Ghamdi, W. E. Mahmoud, S. J. Yaghmour, F. Al-Marzouki, *Journal of Alloys and compounds* **486**: 9. (2009); <https://doi.org/10.1016/j.jallcom.2009.06.139>
- [24] R. Sharma, A. Acharya, S. Shrivastava, et al, *Optik*,. **127**(11), 4661-4668(2016); <https://doi.org/10.1016/j.ijleo.2016.01.050>.
- [25] M. Ghougali, O. Belahssen, S. Benhamida, M. Mimouni, G. Rihia, M. S. Mahboub, A. Beggas, *Chalcogenide Letters* **18** 765. (2021); <https://doi.org/10.15251/CL.2021.1812.765>.
- [26] A. K. Zak, W. A. Majid, M. E. Abrishami, R. Yousefi, *Solid State Sciences*, **13**(1), 251-256 (2011); <https://doi.org/10.1016/j.solidstatesciences.2010.11.024>.
- [27] J. Tauc, *Materials Research Bulletin*, **5**(8), 721-729. (1970); [https://doi.org/10.1016/0025-5408\(70\)90112-1](https://doi.org/10.1016/0025-5408(70)90112-1)
- [28] E. Avendaño, L. Berggren, G. A. Niklasson, C. G Granqvist, A. Azens *Thin solid films*, **496**(1), 30-36. (2006); <https://doi.org/10.1016/j.tsf.2005.08.183>.
- [29] M. B. Amor, A. Boukhachem, K. Boubaker, M. Amlouk *Materials science in semiconductor processing*, 2014. **27**,. 994-1006. (2014); <https://doi.org/10.1016/j.mssp.2014.08.008>.
- [30] A. Beggas, Z. Becer, R. Ahmim, M. S. AIDA, *Defect and Diffusion Forum*, **397**, 125-140 (2019). <https://doi.org/10.4028/www.scientific.net/DDF.397.125>
- [31] F. Urbach, *Physical review*, **92**(5), 1324. (1953); <https://doi.org/10.1103/PhysRev.92.1324>
- [32] P. Patil, L. Kadam, *Applied surface science*, **199**(1-4), 211-221, (2002); [https://doi.org/10.1016/S0169-4332\(02\)00839-5](https://doi.org/10.1016/S0169-4332(02)00839-5)